AGU PUBLICATIONS

JGR

Journal of Geophysical Research: Space Physics

TECHNICAL REPORTS: METHODS

10.1002/2016JA022871

Special Section:
Measurement Techniques in Solar and Space Physics: Optical and Ground-Based

Scientific objectives and capabilities of the Coronal Solar Magnetism Observatory

S. Tomczyk[1], E. Landi[2], J. T. Burkepile[1], R. Casini[1], E. E. DeLuca[3], Y. Fan[1], S. E. Gibson[1], H. Lin[4], S. W. McIntosh[1], S. C. Solomon[1], G. de Toma[1], A. G. de Wijn[1], and J. Zhang[5]

[1]High Altitude Observatory, National Center for Atmospheric Research, Boulder, Colorado, USA, [2]Department of Atmospheric, Oceanic and Space Sciences, University of Michigan, Ann Arbor, Michigan, USA, [3]Harvard–Smithsonian Center for Astrophysics, Cambridge, Massachusetts, USA, [4]Institute for Astronomy, University of Hawai'i at Mānoa, Honolulu, Hawaii, USA, [5]Department of Physics and Astronomy, George Mason University, Fairfax, Virginia, USA

Abstract Magnetic influences increase in importance in the solar atmosphere from the photosphere out into the corona, yet our ability to routinely measure magnetic fields in the outer solar atmosphere is lacking. We describe the scientific objectives and capabilities of the COronal Solar Magnetism Observatory (COSMO), a proposed synoptic facility designed to measure magnetic fields and plasma properties in the large-scale solar atmosphere. COSMO comprises a suite of three instruments chosen to enable the study of the solar atmosphere as a coupled system: (1) a coronagraph with a 1.5 m aperture to measure the magnetic field, temperature, density, and dynamics of the corona; (2) an instrument for diagnostics of chromospheric and prominence magnetic fields and plasma properties; and (3) a white light K-coronagraph to measure the density structure and dynamics of the corona and coronal mass ejections. COSMO will provide a unique combination of magnetic field, density, temperature, and velocity observations in the corona and chromosphere that have the potential to transform our understanding of fundamental physical processes in the solar atmosphere and their role in the origins of solar variability and space weather.

Key Points:
- Society is becoming increasingly vulnerable to the effects of space weather
- The physical processes responsible for solar activity remain poorly understood
- COSMO will provide key measurements to advance our understanding of solar processes and activity

Correspondence to:
S. Tomczyk,
tomczyk@ucar.edu

Citation:
Tomczyk, S., et al. (2016), Scientific objectives and capabilities of the Coronal Solar Magnetism Observatory, *J. Geophys. Res. Space Physics*, *121*, 7470–7487, doi:10.1002/2016JA022871.

Received 25 MAR 2016
Accepted 1 JUL 2016
Accepted article online 7 JUL 2016
Published online 31 AUG 2016

©2016. American Geophysical Union. All Rights Reserved.

1. Introduction

The Earth is inextricably connected to its star. The Sun influences the Earth and the other solar system planets through radiation, particles, and magnetic fields emanating from its atmosphere. Together, these outputs determine the large-scale properties and structure of the heliosphere. Solar outputs are subject to variability due to the continual eruption of magnetic flux into the solar atmosphere that can drive radical disturbances in near-Earth space known as space weather. These disturbances come in the form of coronal mass ejections (CMEs) consisting of large quantities (10^{15}–10^{16} g) of magnetized plasma launched from the solar atmosphere with velocities up to 3000 km/s [*Kahler*, 1992; *Webb and Howard*, 2012], highly variable solar wind, the explosive release of high-energy electromagnetic radiation from flares, and energetic particles from flares and CME-driven shocks. Many critical technologies upon which society has become increasingly dependent are vulnerable to the effects of solar activity. Space weather events have damaged Earth-orbiting satellites, disrupted communications and GPS networks, disabled power grids on the ground, and pose health hazards to astronauts as well as airline passengers on polar routes [*Lambour et al*., 2003; *Iucci et al*., 2006; *Pulkkinen*, 2007; *Schrijver,* 2015].

The physical mechanisms at the Sun giving rise to space weather are poorly understood. How CMEs and flares are energized, what maintains the solar corona at a temperature of several million degrees, how the solar wind is accelerated, and how the composition of the corona is differentiated from that of the photosphere, are all subjects of intense investigation. What is clear is that all of these processes are intricately linked to magnetic fields in the solar atmosphere.

The relative importance of magnetic effects increases with height from gas dominating the force balance in the photosphere to magnetic field dominating the force balance in the corona. Magnetism in the solar photosphere has been increasingly well observed and extensively studied since its discovery [*Hale*, 1908]. Synoptic high-quality observations of photospheric magnetic fields are provided by the space-based Helioseismic and Magnetic Imager (HMI) instrument [*Scherrer et al*., 2012] and ground-based Global Oscillation Network Group [*Harvey et al*., 1996] and Synoptic Long-Term Investigations of the Sun (SOLIS) instruments [*Keller et al*., 2003]. Chromospheric magnetic field observations are much less common than photospheric measurements, with SOLIS providing synoptic chromospheric field measurements. Measurements of magnetic fields in the corona

are rare [*Gary and Hurford*, 1994; *Zhang et al*., 1998; *Lin et al*., 2004; *Brosius and White*, 2006; *Tomczyk et al*., 2008]. We are in the unfortunate situation that the quantity and quality of magnetic measurements in different regions of the solar atmosphere decreases with increasing importance of magnetic influence.

The COronal Solar Magnetism Observatory (COSMO) is a proposed facility designed to measure magnetic fields and plasma properties in the large-scale solar atmosphere. Such measurements have the potential to transform our understanding of fundamental physical processes and their role in the origins of solar variability and space weather. COSMO comprises a suite of instruments chosen to enable the study of the solar atmosphere as a coupled system. This paper presents the scientific motivations for COSMO and provides a description of the instruments designed to address them. The unique capabilities of the COSMO instruments and their role in complementing current and future instruments are described. In addition, the opportunities and challenges that COSMO's combination of observations will pose are discussed. Section 2 presents a discussion of key scientific objectives for COSMO. Section 3 summarizes the measurement requirements. Section 4 provides a description of the instruments in the COSMO suite and their capabilities. Section 5 highlights the uniqueness of the COSMO instruments and how they complement existing and future instruments. Section 6 describes how the COSMO instrument suite will collectively address the science objectives of section 2 and outlines new methodological developments that support and enable COSMO analysis. Section 7 provides an update of the status of COSMO, and concluding remarks are presented in section 8.

2. Scientific Objectives

The COSMO instrument suite is motivated by a number of outstanding questions regarding the Sun. The following is a short description of selected scientific objectives.

2.1. What Is the Evolution of Magnetic and Plasma Properties That Leads to Prominence Eruption and CME Initiation?

Theoretical models and numerical simulations have identified several ways that idealized active region magnetic fields can become unstable and erupt [e.g., *Hood and Priest*, 1981; *Antiochos et al*., 1999; *Roussev et al*., 2003; *Török et al*., 2004; *Kliem and Török,* 2006; *Fan*, 2011]. However, observations that can adequately constrain these models and determine the trigger mechanism are not available. Substantial efforts have gone into developing methods for forecasting solar flares and CMEs using photospheric magnetic field observations. These have afforded an increase in predictive capability over the past decade from a statistical standpoint, but high reliability—especially regarding the timing of future events—is lacking. Correlations have also been found between observed coronal precursor structures and CMEs [*Canfield et al*., 1999; *Forland et al*., 2013], but the usefulness of such observations for space weather forecasting is limited. This problem has been exacerbated by the lack of observations of the magnetic field of the corona, prior to a CME. We understand that CMEs are frequently associated with a particular magnetic structure, namely, the magnetic flux rope, a 3-D current channel with helical magnetic field lines wrapping around its center axial field lines [*Gibson et al*., 2002; *Zhang et al*., 2012], but without direct coronal observations, we cannot address the critical questions: when, where, and how do magnetic flux ropes form, and how do they erupt?

Prominences have long been known to be an important component of space weather, yet their formation, evolution, and the topology of the magnetic field supporting them remain poorly understood. Many CMEs are associated with active and erupting prominences [*Low*, 2001; *Schmieder et al*., 2002; *Gopalswamy*, 2015]. However, vector magnetic field observations in prominences are limited in number [*Bommier et al*., 1994; *Paletou et al*., 2001; *Casini et al*., 2003; *Xu et al*., 2012; *Orozco Suarez et al*., 2014; *Schmieder et al*., 2014]. When viewed with an orientation along the line of sight, prominences are often surrounded by a dark coronal cavity that constitutes the bulk of the erupting CME [*Gibson*, 2015a]. Recent coronal cavity measurements of linear polarization and line-of-sight velocity in the FeXIII 1074 nm line [*Bak-Steslicka et al*., 2013] have indicated a magnetic configuration consistent with flux rope models of pre-CME topologies. Truly distinguishing between magnetic models, however, requires measurement of the line-of-sight magnetic field [*Rachmeler et al*., 2013].

In order to capture and interpret the magnetic signatures of solar eruptions that can be manifested as CMEs, flares, and filament/prominence eruptions, routine observations are needed of the magnetic field, density, and flows in prominences above the limb, as well as measurements of coronal cavity line-of-sight flows

and magnetic fields. This information can be used to determine the structure and evolution of prominence-cavity systems and their role in CME formation.

The heating and acceleration of CME plasmas are also poorly understood. CME plasmas are multithermal (from 0.01 to 10 MK) and rapidly evolving, so their full thermal structure needs to be determined as a function of time. At present, we lack the capability to obtain time series of spectrally resolved 2-D images of the erupting prominence at the CME core, with lines formed at multiple temperatures [*Landi et al*., 2010]. CME models are not constrained because of the lack of adequate observations of CME thermal structures. We also need information on the velocity vectors of ejecta close to the Sun, which is currently lacking. The velocity measurement is useful for inferring the rotation of the erupting flux rope, which takes place during the initial phase of the eruption [*Fan*, 2011] and is important for determining the magnetic field orientation in the resulting interplanetary magnetic clouds.

2.2. What Determines the Magnetic and Thermodynamic Structure of the Corona, and Its Evolution Through the Solar Cycle?

The solar corona is highly structured by magnetic fields at all scales and varies over the solar cycle from a dipole-like configuration during solar minimum to a complex distribution of magnetic field structures at solar maximum. These different configurations determine the structure of the heliosphere and modulate the solar radiative output at UV, EUV, and X-ray wavelengths, with significant effects on the Earth's upper atmosphere [*Gray et al*., 2010]. Current models predict the structure of the solar corona by extrapolating measurements of the photospheric magnetic field into the corona and the heliosphere using a variety of different assumptions and methods [*Schrijver et al*., 2008; *Wiegelmann and Sakurai*, 2012]. However, the highly dynamical state of the solar chromosphere, which is marked by rapid changes of the plasma properties with height above the photosphere, along with the complex nature of magnetic fields and current systems in the corona limits the utility of these extrapolations [*DeRosa et al*., 2009]. Spacecraft have, to some degree, determined the cycle variability of conditions far out in the solar wind. However, we are severely limited in our understanding of how the coronal field responds to the sunspot cycle, largely because of the restricted plasma diagnostic capabilities of EUV and X-ray imagers. Direct measurement of the magnetic and thermodynamic properties of the chromosphere and corona over long time scales are required to characterize the three-dimensional field, its free-energy content, and its evolution, in order to constrain and improve heliospheric models. Measuring the basic structure of the solar magnetic environment will lead to a more complete understanding of solar variability.

Daily solar coronal maps of line-of-sight magnetic field, in combination with white light coronal polarized brightness, are needed to study solar variability over a range of time scales. While such measurements are weighted by the distribution of intensity along the line of sight, as most coronal plasma observations are, much has already been learned by examining the long-term evolution of the white light corona, including solar dipole evolution, north-south hemispheric asymmetries, and the corona-solar wind interface.

For example, the question of magnetic helicity evolution is left unanswered until magnetic field measurements can be made in the corona. This open question is particularly pressing because, if CMEs are important sinks of helicity, then they play a fundamental role in the Sun's cyclic dynamo mechanism [*Low*, 1994]. Addressing the relationship between coronal magnetic fields and the sunspot cycle is an important goal and requires observations with a large field of view and sufficient angular resolution to constrain coronal magnetism and dynamic evolution. On longer time scales, combined white light and coronal magnetic field maps would provide a unique measurement of the solar cycle variation of the global magnetic field.

2.3. How Is the Corona Heated and How Is the Solar Wind Accelerated?

The heating of coronal plasmas is one of the leading open questions in solar physics. Current theories involve nanoflare heating and wave-driven heating, with both having some observational support [*Klimchuk*, 2006; *Aschwanden et al*., 2007]. Recent observations have shown that waves are ubiquitous throughout the chromosphere and corona [e.g., *De Pontieu et al*., 2007; *Tomczyk et al*., 2007; *Morton and McLaughlin,* 2013; *Morton et al*., 2015]. Since heating of the corona and acceleration of the solar wind occur close to the solar surface, observations of the chromosphere and the low corona are critical to understand the physical processes involved. White light coronal images can be used to constrain the 3-D distribution of electron density and morphology of the large-scale corona over time. However, white light images provide no

thermodynamic and element composition information that are required to understand how coronal heating evolves through the solar cycle. Eclipse observations of a number of emission lines formed at different temperatures have demonstrated their utility for studying the thermodynamics of the corona [e.g., *Habbal et al*., 2011]. Routine observations of many spectrally resolved emission lines from plasmas between 0.01and 5 MK over a large field of view could be used to infer the 3-D distribution of the emission and the abundance of the same ions later observed in the solar wind by mass spectrometers. These will also help determine the 3-D thermal structure of the entire corona and follow its evolution with the solar cycle.

Spectroscopic observations of multiple lines emitted at different temperature ranges would allow us to establish the relationship of Alfvén waves to plasma structures and their thermal distribution and to assess the role of nanoflares in the heating of coronal magnetic field structures. Such a relationship needs to be investigated along the solar cycle in order to establish whether the Alfvén wave properties, nanoflare heating, and coronal heating depend on solar cycle phase and strength. Furthermore, measurements of the coronal magnetic field are essential to make quantitative connections to in situ measurements of solar wind conditions (e.g., by the NASA Solar Probe Plus mission).

2.4. How Can We Improve Space Weather Predictions?

One of the most important applications of solar coronal physics is to provide timely and accurate prediction of space weather events in order to mitigate their adverse effect on human technology and society. Prediction of solar events would be enabled by identifying precursors of both flares and CMEs. Photospheric magnetic fields do not show any obvious changes preceding these events. This implies that flares and CMEs are powered by the release of energy stored in coronal magnetic fields. Therefore, it is realistic to expect that the latter may experience measurable changes prior to these events; also, they can be used to monitor energy buildup in magnetic structures that can lead to their destabilization. State-of-the-art space weather prediction models rely on the specification of coronal magnetic free energy and 3-D topology, but these are largely unconstrained by observations. Accurate 3-D coronal magnetic field maps would provide the critical inner boundary condition for any space weather prediction system. They would support simulations of the slowly evolving ambient solar wind across the heliosphere that are needed for predicting the arrival times at Earth of CMEs, corotating interaction regions, and interplanetary shocks that propagate through and interact with the solar wind [*Pizzo et al*., 2011]. Current numerical modeling systems usually adopt extrapolations of coronal magnetic fields based on photospheric field measurements. These extrapolated fields cannot accurately reproduce the nonpotential fields present in the corona resulting in poor predictions of trajectory and arrival times of CMEs that can cause false alarms and missed predictions of space weather events.

Coronal field observations will need to be accompanied by model development to improve space weather prediction capability. Ultimately, the goal will be to utilize coronal magnetic and thermodynamic data in solving the nonlinear inverse problem for the full three-dimensional magnetic field. For localized coronal loop source regions, a single-point inversion is possible, as demonstrated for combined FeXIII 1074.7 and 1079.8 nm observations [*Plowman*, 2014]. Another approach that is not limited to a localized source is tomography where observations along multiple lines of sight are analyzed to yield a spatially varying distribution of the desired physical quantity. Solar coronal density and temperature distributions have been reconstructed using these methods, employing either solar rotation or the STEREO spacecraft viewpoints to define multiple lines of sight [*Frazin et al*., 2007; *Kramar et al*., 2014]. The more difficult problem of tomographically reconstructing the vector magnetic field from polarization measurements has recently been studied for FeXIII forbidden lines [*Kramar et al*., 2006, 2013, 2016]. Another approach to reconstructing the coronal magnetic field utilizes the photospheric magnetic field as a boundary but adjusts the distribution of currents to match coronal observations [*Savcheva and van Ballegooijen*, 2009; *Malanushenko et al*., 2012]. This type of forward fitting approach has the possibility of incorporating information from multiple viewpoints or solar rotation in a manner akin to tomography as well as from localized loop inversions or prominence magnetic field measurements incorporated as a priori constraints. Moreover, it is straightforward to extend it to incorporate a range of data, such as multiwavelength spectroscopic and polarimetric coronal measurements, into a combined quantity to be globally minimized. Such multiwavelength measurements differ in their sensitivity to temperature and magnetic field strength and so probe different parts of the corona. Coronal limb observations (white light and spectropolarimetric) could be used in conjunction with chromospheric disk observations as part of a forward fit, to yield a comprehensive, data-constrained model of the full 3-D coronal magnetic field.

Table 1. COSMO Science Traceability

Scientific Objectives	Measurement Objectives	Measurement Requirements	Instrument Requirements
2.1 What is the evolution of magnetic and plasma properties that leads to prominence eruption and CME initiation?	prominence magnetic field and velocity	magnetic sensitive chromospheric lines, 1 G *B* field sensitivity, 2 arc sec resolution, 1 km/s velocity sensitivity, large FOV, synoptic	spectropolarimetric imaging, 0–1.25 Rsun FOV, 550–1100 nm wavelength range, 23,500 spectral resolution, 0.15 m aperture
	coronal magnetic field and velocity	1 G *B* field sensitivity in 15 minutes and 2 sec resolution, 1 km/s velocity sensitivity, large FOV, synoptic	spectropolarimetric imaging, 1.05–2 Rsun FOV (coronagraph), 500–1100 nm wavelength range, 8000 spectral resolution, 1.5 m aperture
	coronal temperature and density	coronal lines formed at different temperatures, density sensitive line pairs, large FOV, synoptic	spectroscopic imaging, 1.05–2 Rsun FOV (coronagraph), 500–1100 nm wavelength range
	coronal electron density	pB measurement, 15 s cadence, large FOV, synoptic	*K*-coronagraph with 1.05–3 Rsun FOV
2.2 What determines the magnetic and thermodynamic structure of the corona, and its evolution along the solar cycle?	coronal temperature and density distribution	coronal lines formed at different temperatures, density sensitive line pairs	spectroscopic imaging, 1.05–2 Rsun FOV (coronagraph), 500–1100 nm wavelength range
	coronal magnetic field	1 G *B* field sensitivity, large FOV, daily cadence	spectropolarimetric imaging, 1.05–2 Rsun FOV (coronagraph), 500–1100 nm wavelength range, 1.5 m aperture
	chromospheric and prominence magnetic fields	magnetic sensitive chromospheric lines, 1 G *B* field sensitivity, large FOV, synoptic	spectropolarimetric imaging, 0–1.25 Rsun FOV, 550–1100 nm wavelength range, 0.15 m aperture
	coronal electron density	pB measurement, large FOV, synoptic	*K*-coronagraph with 1.05–3 Rsun FOV
2.3 How is the corona heated and how is the solar wind accelerated?	coronal and chromospheric wave properties	intensity and Doppler observations, 30 second time cadence, 100 m/s velocity sensitivity, large FOV, synoptic	spectroscopic imaging, 0–1.1 Rsun FOV (chromospheric imager), 1.05–2 Rsun FOV (coronagraph)
	coronal magnetic field	1 G *B* field sensitivity in 15 min and 2 arc sec resolution, large FOV, synoptic	spectropolarimetric imaging, 1.05–2 Rsun FOV (coronagraph), 1.5 m aperture
	coronal temperature and density distribution	coronal lines formed at different temperatures, density sensitive line pairs	spectroscopic imaging, 1.05–2 Rsun FOV (coronagraph), 500–1100 nm wavelength range
2.4 How can we improve space weather prediction?	coronal magnetic field	1 G *B* field sensitivity, large FOV, synoptic	spectropolarimetric imaging, 1.05–2 Rsun FOV (coronagraph), 1.5 m aperture
	coronal temperature and density distribution	coronal lines formed at different temperatures, density sensitive line pairs, large FOV, synoptic	spectroscopic imaging, 1.05–2 Rsun FOV (coronagraph), 500–1100 nm wavelength range
		model development	

3. Required Measurements

These scientific objectives dictate a set of requirements on the measurements needed to address them. Table 1 summarizes the flow down from science questions to measurement and instrument requirements. All of the science questions from above require synoptic observations of the large-scale solar atmosphere on time scales ranging from 15 s to a solar cycle. The field of view must be sufficient to encompass large coronal loop, prominence, cavity, and streamer systems and to allow tracking of CME ejecta. This can be achieved with a field of view of 1° for the corona; a somewhat smaller field of view is adequate for chromospheric and prominence observations. Any instrument is limited in the number of spatial elements it can acquire, and this inevitably leads to a tradeoff between spatial resolution and field of view. The 4 m aperture Daniel K. Inouye Solar Telescope (DKIST) [*Keil et al.*, 2003] and missions like the Hi-C rocket experiment

[*Kobayashi et al.*, 2014] are designed to achieve the highest possible spatial resolution. This capability comes at a price of having a restricted field of view; the Hi-C field of view is 5.5 arc min and the DKIST field of view is 5 arc min. The COSMO instruments will be complementary to DKIST and Hi-C and provide large field-of-view observations of the solar corona with 2 arc sec spatial resolution and an emphasis on a synoptic mode of operation that is matched to the key physical processes controlling space weather. A reasonable requirement is to provide spatial resolution comparable to instruments like the Transition Region and Coronal Explorer [*Handy et al.*, 1999] and the Atmospheric Imaging Assembly (AIA) [*Lemen et al.*, 2012] that have been able to address a wide range of coronal problems. The science questions can be addressed with a spatial resolution of 2 arc sec. Measured quantities include the coronal magnetic field strength and orientation, velocity, temperature, density and intensity, the chromospheric and prominence vector magnetic and velocity fields and intensity, and the coronal electron density. The coronal magnetic field measurements need a sensitivity of 1 G with a range up to several kilogausses to allow measurement of both quiet and active region coronal fields. A similar range on the prominence magnetic field is required. Spectral resolution sufficient to resolve the polarization signature in the Stokes circular polarization profile and Doppler shifts is required. For coronal emission lines, this corresponds to a resolution $\lambda/\Delta\lambda > 8000$ [*Tomczyk et al.*, 2016]. The velocity sensitivity of 100 m/s is dictated by the need to observe waves in the corona and chromosphere at a cadence of 30 s. And the need for temperature and density diagnostics in the corona and chromosphere drive the requirement for observations over a wavelength range sufficient to capture emission lines formed over a range of temperatures and density sensitive line pairs to derive densities.

This set of requirements is impossible to meet with a single instrument. This has led to the development of a suite of three complementary instruments to address them; these are described in the next section.

4. The COSMO Suite of Instruments

The science questions and the instrument requirements they drive can be addressed with a suite of three synoptic ground-based telescopes working in unison. COSMO comprises (1) a large coronagraph (LC) with a 1.5 m aperture to measure the magnetic field, temperature, density, and dynamics of the corona; (2) an instrument for monitoring chromosphere and prominence magnetic fields and plasma properties (ChroMag); and (3) a white light K-coronagraph (K-Cor) to measure the density structure and dynamics of the corona and CMEs. The LC will be a stand-alone instrument, while the K-Cor and ChroMag will reside on a separate solar pointed spar.

In this section, the capabilities of these instruments are described in relation to the requirements discussed in the previous section. Technical details of the design of these instruments will be given in separate publications.

4.1. Large Coronagraph (LC)

The measurement methodology for the COSMO LC follows from a comprehensive overview of available methods [*Judge et al.*, 2001] that identified the Zeeman and resonance scattering polarization effects as the most promising methods to measure magnetic fields in the corona. The line-of-sight strength of coronal magnetic fields can be measured directly through the Zeeman effect observed in the circular polarization of coronal forbidden emission lines. The linear polarization from resonant scattering of photospheric radiation is used to measure the plane-of-sky direction of the magnetic field. These measurement techniques have a dynamic range from a fraction of a Gauss to several thousand Gauss; this is critical to provide information on both large-scale "quiet" coronal fields and active region fields.

Observing the Zeeman effect in the solar corona is challenging. The corona is 5 to 6 orders of magnitude fainter than the solar photosphere; coronal magnetic fields away from active regions are weak, of order 1–10 Gauss, and the emission lines are thermally broadened by the million degree plasma. The expected error in the magnetic field strength can be estimated through propagation of errors to be

$$\sigma_B = \frac{16.5}{\sqrt{N}}\left(1 + 2\frac{B}{N}\right)^{1/2} (\mathrm{kG}) \tag{1}$$

[*Penn et al.*, 2004; *Tomczyk*, 2015], where N is the number of photons integrated over the emission line and B is the number of photons in the background over the same wavelength interval. This equation assumes a single beam polarimeter with a polarimetric efficiency of 0.57. The noise scales inversely as the square root of the number of photons in the usual way but also includes the term in brackets that represents the penalty

Table 2. Candidate Visible and Near-IR Lines That Will be Observed by the COSMO LC[a]

CME Core		CME Hot Component		Quiescent Corona	
Line	log T_{eff}	Line	log T_{eff}	Line	log T_{eff}
HI 656.3	4.01–4.29	FeXIV 530.3	6.15–6.49	FeX 637.5	5.80–6.24
HeI 587.6	4.01–4.57	FeXV 706.2	6.20–6.63	FeXI 789.2	5.92–6.30
HeI 1083.0	4.01–4.57	SXII 761.1	6.16–6.55	FeXIII 1074.7 (N_e)	6.08–6.41
CaII 854.2	4.01–4.34	ArXIII 830.0 (N_e)	6.26–6.67	FeXIII 1079.8(N_e)	6.08–6.41
OII 732.1	4.16–4.92	ArXIII 1014.3 (N_e)	6.26–6.67	FeXIV 530.3	6.15–6.49
OII 733.2	4.16–4.92	CaXV 544.5 (N_e)	6.44–6.84	ArX 552.2	5.86–6.42
OIII 500.8	4.62–5.23	CaXV 569.4 (N_e)	6.44–6.84	ArXI 691.8	6.04–6.52
FeVI 520.0	4.95–5.52				

[a]Wavelengths are in nanometers. Lines from the same ion indicated with (N_e) provide density sensitive line pairs. log T_{eff} indicates the temperature range where each ion has fractional abundance 0.01 or larger under equilibrium conditions.

on the noise due to background photons from the sky and instrumental scattering. Equation (1) was derived assuming observation of the FeXIII emission line at 1074.7 nm; this line has the highest expected signal-to-noise ratio of all known coronal emission lines [*Judge et al*., 2001]. This equation illustrates the difficulty of this measurement. Even for the case of negligible background ($B = 0$), 2.7 x 10^8 photons are required to achieve 1 G precision. In order to collect enough photons to measure the coronal magnetic field strength with a sensitivity of 1 G, in 15 min, with 2 arc sec spatial resolution drives the need for a telescope with an aperture of 1.5 m (assuming a coronal brightness of 10 ppm of the solar disk intensity, a background of 5 ppm, and a dual-beam polarimeter).

To achieve a low level of background light and minimize the penalty on the noise, a coronagraph located at a site with very dark sky is needed. Scattered-light analysis of reflecting and refracting coronagraph objectives shows that lenses scatter significantly less light than mirrors from the effects of both surface roughness and dust contamination [*Nelson et al*., 2008]. For this reason, we have selected a lens for the objective of the COSMO LC. It is likely that dust on the objective will be the dominant source of scattered light. To mitigate this, the LC dome will have a minimally sized aperture and the dome will be pressurized with filtered air.

The COSMO LC derives its heritage from prototype instruments that have successfully demonstrated the feasibility of the proposed measurement techniques: the University of Hawaii Optical Fiberbundle Imaging Spectropolarimeter [*Lin et al*., 2004] and the High-Altitude Observatory (HAO)/National Center for Atmospheric Research (NCAR) Coronal Multichannel Polarimeter (CoMP) [*Tomczyk et al*., 2008]. These efforts have been enabled by recent advances in detector technology that make possible the observation of near-IR emission lines that are highly sensitive to the Zeeman effect. However, these prototype instruments are severely limited by the modest apertures of the available coronagraphs.

The COSMO Large Coronagraph is proposed to have the following characteristics to meet the science objectives: (1) internally occulted Lyot coronagraph with 1.5 m diameter lens; (2) field of view of 1°; (3) 2 arc sec spatial resolution; (4) spectral resolution $\lambda/\Delta\lambda > 8000$; (5) wavelength range from 500 to 1100 nm; (6) coronal magnetic field sensitivity of 1 G in 15 min; (7) cadence of 1 s for intensity and Doppler measurements.

The aperture of the LC is driven by the need to collect sufficient photons to achieve the magnetic field sensitivity for the Zeeman measurements. The 1° field of view allows the study of typical large-scale coronal structures. The broad wavelength range is critical to observe many visible and near-IR emission lines over a range of formation temperatures between 0.01 to 5 MK and to observe line pairs at several temperatures for line-ratio density diagnostics. Candidate lines for the COSMO LC are shown in Table 2. The spectral resolution is chosen to be able to resolve the Zeeman and Doppler signatures of the emission lines. The large aperture will allow a temporal cadence of 1 s for intensity and Doppler measurements, exceeding the 30 s cadence requirement, and will allow critical observations of coronal MHD waves and turbulence and the ability to follow coronal dynamics. Observation of other lines in the wavelength range 500–1100 nm is possible; this wavelength range is limited by the transmission range of the tunable filter. The fused silica objective lens of the coronagraph transmits light in the wavelength range 200 to 2200 nm. The LC is designed to allow the postfocus instrument to be easily replaced or upgraded. Rendering of the COSMO LC dome and telescope is shown in Figure 1. The field of view of the LC is illustrated in Figure 2. For synoptic operation, the LC will be

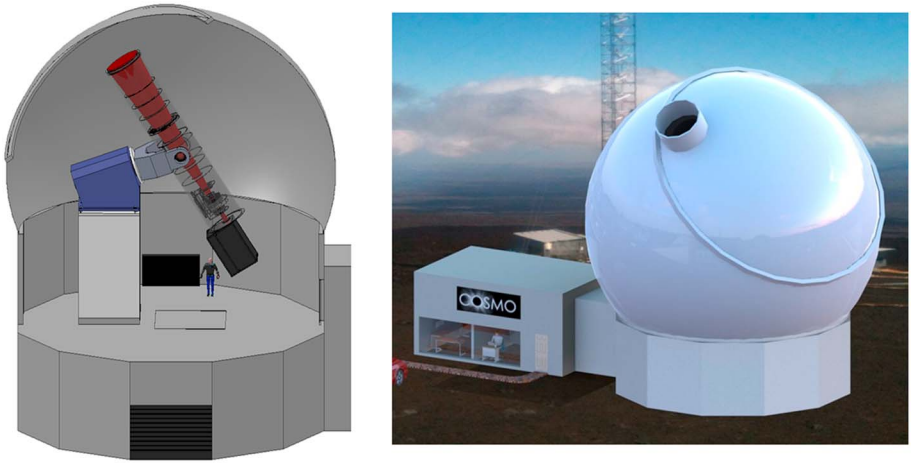

Figure 1. (left) Cutaway rendering showing the inside of the COSMO LC dome with the coronagraph and postfocus instrument. (right) Rendering of the exterior of the LC facility showing the control building and fifth/eighth's dome with minimum-sized aperture.

pointed in a Sun-centered configuration. However, to respond to solar events, it will be possible to position the LC field of view out to the solar limb, as shown in the right panel of Figure 2.

A key enabling technology for the LC is the postfocus tunable filter. It must provide a spectral resolution greater than 8000 over the 500–1100 nm wavelength range across the 1° field of view. The product of the solid angle field of view and the area of the entrance pupil is called the étendue [*Jacquinot*, 1954], which determines the light gathering power of a telescope. To avoid light losses, the étendue must be conserved through the postfocus optical system. To accept the beam from the 1.5 m diameter LC with a 1° field of view, the 100 mm diameter postfocus tunable filter must be able to accept a 15° field of view. This is extremely challenging since the central wavelength of the filter passband must shift by less than 0.1 of the filter bandwidth and the transmission profile must not broaden appreciably over this angular range. We find that a wide-field birefringent filter made with Lithium Niobate crystals can meet the étendue requirement of the LC tunable filter. The development of this filter is described in detail in a separate publication [*Tomczyk et al.*, 2016].

Polarization analysis will be accomplished by a rotating waveplate followed by a polarizing beamsplitter. This dual-beam technique will allow the simultaneous measurement of orthogonal polarization states which is important to eliminate seeing induced noise in the polarization measurement.

4.2. Chromosphere and Prominence Magnetometer (ChroMag)

Chromospheric observations provide important information on plasma conditions in the low atmosphere which are needed to bridge observations of the photosphere to those of the corona. Measurements of

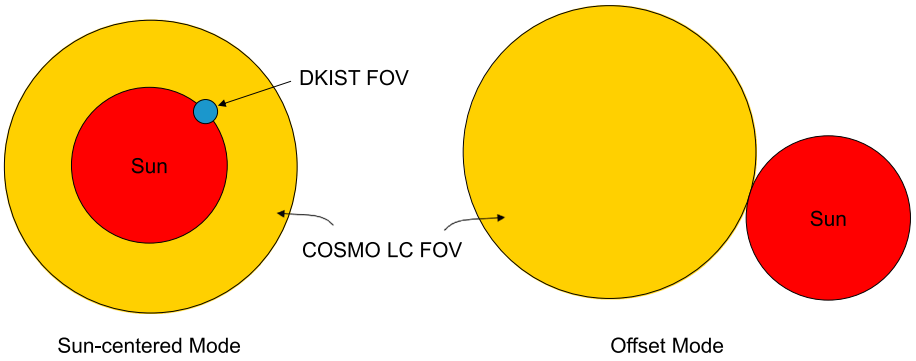

Figure 2. (left) Illustration of the field of view of the COSMO LC (orange, 1.0°) for the Sun-centered pointing mode. The field of view of the DKIST (blue, 5 arc min) and the size of the Sun (red, 0.53°) are shown for comparison. (right) Illustration of the offset pointing mode for the LC.

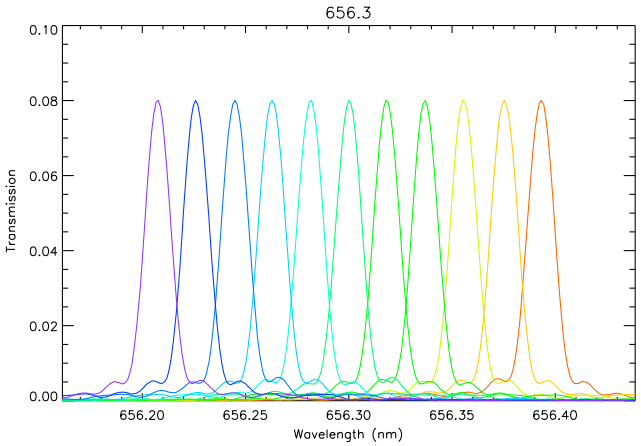

Figure 3. The measured transmission profiles for the ChroMag electro-optically tunable filter in the vicinity of 656.3 nm. The transmission profiles for 11 tunings offset by 19 pm are shown by the different colors and superimposed.

prominence fields are rare but have been obtained using the Hanle effect [e.g., *Leroy et al.*, 1984; *Querfeld et al.*, 1985; *Bommier et al.*, 1994; *Paletou et al.*, 2001; *Casini et al.*, 2003; *Merenda et al.*, 2006; *Orozco Suarez et al.*, 2014]. This research has determined that the optimal lines for examining magnetic fields in prominences are the HeI 587.6 and 1083.0 nm lines. The HI line at 656.3 nm has been widely used historically as a diagnostic for chromospheric structure and dynamics. The well-known CaII line at 854.2 nm samples chromospheric magnetic field and structure in its core, while its wide wings provide a diagnostic of the atmosphere down to the photosphere. Finally, a photospheric diagnostic is useful for cross calibration and alignment with existing photospheric magnetometers. The FeI line at 617.3 nm is a good choice due to its use by the HMI instrument on board Solar Dynamics Observatory [*Scherrer et al.*, 2012]. An important consideration is that the sound speed is an order of magnitude higher in the chromosphere than in the photosphere; chromospheric measurements need to be taken at a higher cadence than photospheric measurements in order to capture waves and dynamics.

These considerations drive the requirements for the second instrument in the COSMO suite, ChroMag, an imaging polarimeter for magnetic and plasma diagnostics of the chromosphere and prominences. The ChroMag will utilize a telescope and tunable filter to measure the polarization and Doppler shift of chromospheric, prominence, and photospheric lines [*de Wijn et al.*, 2014].

The optical system for the ChroMag instrument consists of a doublet objective lens, a field lens, a narrowband tunable filter, a reimaging lens, and a detector. The tunable filter is a wide-field birefringent filter [*Lyot*, 1933; *Evans*, 1949] comprised of six stages; each stage consists of an entrance polarizer, a calcite waveplate, an achromatic half waveplate, another calcite waveplate, a nematic liquid crystal variable retarder, and an exit polarizer. The length of the calcite crystals is doubled in each stage in the usual manner and the linear polarizers are shared by adjacent stages. The thickest stage contains two calcite crystals 44 mm thick. The wavelength of the passband is tuned by changing the voltage applied to the liquid crystals. Figure 3 shows an example of the passbands tuned in this way in the vicinity of the HI 656.3 nm line. Figure 4 shows the full width at half maximum (FWHM) spectral resolution provided by the filter and the free spectral range between successive orders of the transmission that must be blocked by interference filters. The ChroMag polarimeter precedes the tunable filter and is integrated into the same package as the tunable filter. It consists of two ferroelectric liquid crystals followed by a retarder; the first polarizer for the tunable filter acts as the analyzing polarizer for the polarimeter. The polarimeter performs a full Stokes analysis of the incoming beam. It operates over the 587 to 1083 nm wavelength range as a polychromatic polarimeter [*Tomczyk et al.*, 2010] where the modulation properties of

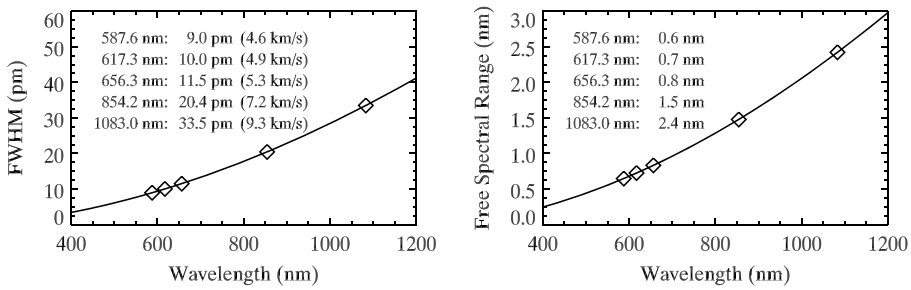

Figure 4. (left) The pass band FWHM and (right) the free spectral range of the ChroMag tunable filter.

the polarimeter vary but remain nearly optimal over the wavelength range. Polarization calibration standards are inserted into the beam and rotated to calibrate the properties of the polarimeter. Both the filter wavelength tuning and the polarization analysis are accomplished electro-optically and require no moving parts.

ChroMag has the following characteristics (1) 15 cm aperture telescope with tunable filter/polarimeter; (2) field of view of 2.5 solar radii including full solar disk and above the limb; (3) spatial resolution of 2 arc sec; (4) spectral coverage including HeI (587.6 and 1083 nm) for prominences, HI (656.3 nm) and CaII (854.2 nm) for the chromosphere and FeI (617.3 nm) for the photosphere; (5) filter bandwidth ranging from 0.025 nm in the visible region to 0.046 nm in the IR provides magnetic field, Doppler, and line width; (6) polarimetric sensitivity of 10^{-3} in 1 min per line; and (6) temporal cadence of 10 sec per line for intensity and Doppler observations of MHD waves.

The aperture of ChroMag provides the required spatial resolution and flux levels to meet the polarimetric sensitivity requirement. The spectral resolution for ChroMag was set by simulating the observation and inversion of polarized line profiles of prominences in the presence of noise. These indicated that magnetic fields could be recovered with a filtergram instrument if the filter bandwidth is 25 pm or less for the HeI 587 nm line, 46 pm or less for the HeI 1083 nm line, and the polarimetric accuracy exceeds 10^{-3} [*Casini*, 2007]. The FWHM bandwidth and the free spectral range of the ChroMag filter are shown in Figure 4. The ChroMag spectral resolution is sufficient to measure Doppler shifts and line widths and to infer vector magnetic fields via full Stokes polarimetry. The temporal cadence of 10 s is sufficient to observe waves in the chromosphere, which may be an important source of energy to heat the chromosphere and corona.

4.3. K-Coronagraph (K-Cor)

Coronal broadband "white light" observations provide important data on the basic properties of CMEs such as size, mass, speed, and acceleration [*Howard et al*., 1985; *Hundhausen*, 1993; *St. Cyr et al*., 1999; *MacQueen et al*., 2001]. The K-Cor is a white light coronagraph that observes the polarization of coronal light in the continuum providing a direct measurement of the column density of coronal electrons which is independent of thermodynamic factors. The K-Cor is the one component of the COSMO suite that is already operational. K-Cor went into service in September 2013 at the Mauna Loa Solar Observatory, replacing the MkIV coronameter [*Elmore et al*., 2003] that was an upgrade to the MkIII coronameter [*Fisher et al*., 1981]. The K-Cor observes the linearly polarized component of continuum light in a 35 nm wide bandpass centered at 735 nm. The dual-beam optical system images the orthogonal linear polarization states simultaneously in order to cancel noise in the polarization measurement caused by seeing and intensity variations from the passage of aerosols through the field of view. The K-Cor is able to achieve instrumental scattering below 5 ppm by employing a superpolished objective lens and HEPA filtering for dust control. A description of K-Cor was given by *de Wijn et al.* [2012].

The characteristics of the K-Cor are the following: (1) 20 cm aperture internally occulted coronagraph with linear polarization analysis; (2) field of view from 1.05 to 3 solar radii; (3) spatial sampling of 6 arc sec per pixel; (4) temporal cadence of 15 s; and (5) sensitivity of 10^{-9} of the disk center intensity.

The K-Cor full field of view of 6 solar radii is needed for observing the density structure of the global corona and for measuring the properties of dynamic events such as CMEs. The large field of view and high time cadence allows K-Cor to adequately sample the plane-of-sky velocity and acceleration profiles and expansion rates of CMEs. The lower limit of the field of view is 1.05 solar radii; it provides the first routine white light measurements of the lowest coronal scale height where most CMEs originate and are accelerated.

The observing cadence of K-Cor of 15 s is rapid enough to detect and follow the dynamical processes of CME initiation, prominence eruption/rotation, magnetic reconnection, wave propagation, and shock formation. Time scales of 30 min to an hour are sufficient for studying the evolution of large-scale coronal structures. The lower noise level and larger field of view will enhance the ability of K-Cor to observe halo CMEs over that of its predecessor, the MkIV coronagraph. Observations from K-Cor are illustrated in Figure 5. K-Cor observations are available from the Mauna Loa Solar Observatory website: http://www2.hao.ucar.edu/mlso/mlso-home-page.

5. COSMO Uniqueness and Complementarity

The COSMO suite will provide a unique set of measurements that will complement observations obtained from other instruments on the ground and from space.

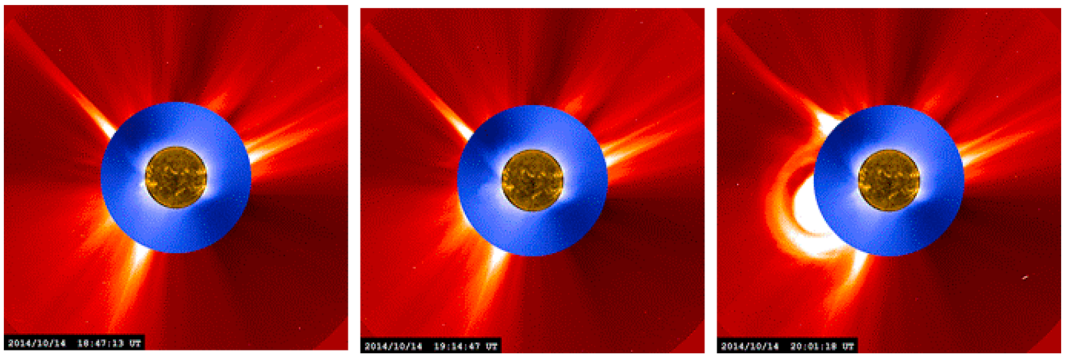

Figure 5. CME observed on 14 October 2014 in AIA (gold), the *K*-Cor (blue) and LASCO C2 (red). The *K*-Cor observed the start of the CME ~20 min before Large Angle and Spectrometric Coronagraph (LASCO) and provides observations of the rapid expansion and acceleration of the CME from its formation to the C2 FOV.

5.1. Large Coronagraph

While much continues to be learned about the solar corona through observations with space-based EUV imagers and spectrographs, the COSMO LC will provide valuable complementary information. EUV imagers like AIA employ filters that are much wider than the emission lines they observe. This lack of spectral information precludes the measurement of Doppler shifts and line widths and allows unwanted contamination by nearby lines severely impacting the temperature resolution. EUV spectrographs like the Hinode EUV Imaging Spectrometer [*Culhane et al*., 2007] and the Interface Region Imaging Spectrograph (IRIS) [*De Pontieu et al*., 2014] have the ability to spectrally resolve individual emission lines, but the field of view of these instruments is limited and they are unable to observe quickly evolving phenomena like CMEs and MHD waves and to obtain simultaneous coverage of the large-scale corona. In addition, since the Zeeman splitting scales as wavelength squared, the coronal magnetic field is extremely difficult or impossible to measure at EUV wavelengths. Hanle diagnostics are available at these wavelengths, but they are sensitive only over a restricted range of field strength. At EUV wavelengths, even Doppler shifts are difficult to observe with sufficient accuracy to measure the properties of Alfvén waves. Also, radiation from EUV lines is typically determined by collisional processes that scale as electron density squared, while the emission from visible lines are dominated by radiation and scales as the electron density. This means that EUV emission lines decrease in intensity with height much faster than visible and IR lines making them more difficult to observe to large heights above the limb. COSMO LC observations are then very complementary to EUV observations in that they will provide emission line intensity, spectral diagnostic information, and polarization analysis at high cadence over a 1° field of view.

The importance of the large field of view of the LC cannot be overstated. The Daniel K. Inouye Solar Telescope (DKIST) [*Keil et al*., 2003] is a 4 m aperture solar telescope currently under construction that has the ability to measure coronal magnetic fields above the limb using the same Zeeman and scattering polarization diagnostics as the COSMO LC. Due to its large aperture, the DKIST is optimized for high spatial resolution observations over a maximum 5 arc min field of view (shown in Figure 2). The light gathering ability of a telescope is given by the product of the area of the collecting aperture and the solid angle of the field of view. While DKIST has a factor of 7 greater collecting area, that advantage is more than compensated by the factor of 144 larger solid angle of the COSMO LC. The LC will have a light gathering power that exceeds that of the DKIST by a factor of 20. The user-driven observing mission and high spatial resolution capabilities of DKIST are complementary to the synoptic mission and large field-of-view measurements provided by the COSMO LC. The LC is optimized for observation of the corona over a range of spatial and temporal scales that will not be available to the DKIST.

Radio techniques can also be used to obtain information on magnetic fields in the corona, since the opacity and polarized plasma emission at radio wavelengths is sensitive to the strength and geometry of the magnetic field through a variety of mechanisms [*Dulk and McLean*, 1978; *White*, 2005]. The two primary mechanisms are *gyroresonance*, which is sensitive to the strength of strong magnetic fields ($>$100 G) above active regions and operates both on the disk and above the limb [*White and Kundu*, 1997; *Brosius and White*,

2006], and *bremsstrahlung*, that can used to measure weak quiet sun magnetic fields in both optically thin [*Bogod and Gelfreikh*, 1980] and optically thick regimes [*Grebinskij et al*., 2000]. In addition, Faraday rotation of polarized radiation from background sources can be used to infer the coronal magnetic field [*Alissandrakis and Chiuderi-Drago*, 1995; *Jensen et al*., 2013]. Radio methods have strengths and weaknesses compared to the visible and IR methods to be used by COSMO and DKIST. The vastly different dependences on temperature, density, filling factor, geometry of the magnetic field, and line-of-sight integration between the various methods makes the radio measurements valuable complements to the visible and IR methods. Future progress of coronal magnetometry at radio wavelengths will be accomplished by the Very Large Array, the Atacama Large Millimeter Array [*Wedemeyer et al*., 2015], the Expanded Owens Valley Solar Array under construction, the proposed Frequency Agile Solar Radiotelescope [*Bastian*, 2003], and the Chinese Spectral Radio-Heliograph [*Yan et al*., 2009].

5.2. ChroMag

Other instruments will provide observations that complement the information that will be provided by ChroMag. The SOLIS Vector Spectromagnetograph (VSM) [*Keller et al*., 2003] makes regular observations in the chromospheric CaII 854.2 nm and HeI 1083.0 nm lines with high spectral resolution. However, the VSM only measures intensity in both lines and circular polarization in CaII 854.2 nm, yielding just a line-of-sight field strength. Furthermore, since it is a slit-scanning spectrograph, the cadence of the observations is too slow to study the dynamics of the chromosphere, waves, and transient events like flares.

The IRIS instrument [*De Pontieu et al*., 2014] observes the chromospheric lines of MgII h and k in the UV, as well as photospheric and coronal lines at subarcsecond spatial resolution with 2 s temporal resolution over a field of view of 175 × 175 arc sec. The IRIS provides a wealth of information but does not include polarimetry and cannot measure magnetic fields.

The Interferometric Bidimensional Spectrometer [*Cavallini*, 2006] instrument at the Dunn Solar Telescope at Sac Peak is an imaging polarimeter and has capabilities similar to ChroMag, except that it is not a synoptic instrument and its field of view is much smaller than that of ChroMag, about 80 arc sec. Likewise, the CRisp Imaging SpectroPolarimeter [*Scharmer*, 2006] at the 1 m Swedish Solar Telescope on La Palma provides a complementary high spatial resolution, nonsynoptic complement to the ChroMag capabilities.

ChroMag will provide routine observations of the vector magnetic field and flows in the chromosphere and prominences. Its large field of view with Doppler and polarization imaging capabilities with high temporal cadence make it unique and highly complementary to these instruments.

5.3. K-Coronagraph

The K-Cor is unique as the only ground-based white light coronagraph and the sole source of white light observations of the corona below 1.5 solar radii. The K-Cor provides an important complement to space-based coronagraphs such as SOHO/Large Angle and Spectrometric Coronagraph (LASCO) [*Brueckner et al*., 1995] and STEREO Cor1 [*Thompson et al*., 2003] that observe only down to 2 solar radii (LASCO C2) and 1.5 solar radii (Cor1). Low coronal observations from the K-Cor are uniquely capable of filling the gap between space-based observations of the low corona at EUV and X-ray wavelengths and white light observations of the outer corona provided by SOHO/LASCO and STEREO.

6. COSMO Enabling Science

The COSMO suite of instruments will work in synergy to address the scientific objectives described in section 2. COSMO opens entirely new windows to study and model CMEs. First, by measuring the magnetic field in the corona and in prominences, COSMO can constrain the magnetic structure and topology of CME precursors such as filament channels and prominence-cavity systems and measure their dynamic properties during the onset of eruption. Second, by fully resolving coronal emission lines sampling the 0.01–5 MK range, it allows the complete determination of the thermal energy budget of all CME components during onset: erupting prominence, reconnected plasma, and current sheet. Observation of coronal density sensitive line ratios at several temperatures combined with electron density measurements from K-Cor will lead to improved estimates of CME density and mass. CMEs are easily observed in Doppler and line width data obtained with the CoMP instrument [*Tian et al*., 2013], and shocks have been observed in white light polarization [*Vourlidas et al*., 2003]. By combining plane-of-sky motions from K-Cor and Doppler shifts from

ChroMag and LC, COSMO will provide the first ever continuous measurements of 3-D velocity of the entire CME during onset.

COSMO will make it possible to associate direct magnetic field measurements with plasma properties across the whole solar atmosphere and monitor them for long periods of time. The ground-based location of COSMO ensures easy maintenance and upgrades allowing for operation over multiple solar cycles, while the synoptic nature of COSMO will provide a continuous set of standard daily data products (weather permitting) from its suite of instruments on the magnetic, thermodynamic, density, and dynamic state of the solar atmosphere. These will address how the chromosphere and corona drive the evolution of the heliosphere on solar cycle timescales and will elucidate the role of CMEs in the balance of solar helicity.

The COSMO LC will improve on measurements of coronal MHD waves from CoMP [*Tomczyk and McIntosh*, 2009] with better temporal and spatial resolution using emission lines formed over a wide range of temperatures. Combining the coronal measurements with chromospheric wave measurements from ChroMag will allow study of the energy coupling of these atmospheric regions and enable study of the role of waves in chromospheric and coronal heating over a wide range of spatial scales. Characterization of MHD waves also provides an additional powerful diagnostic of magnetic fields through seismological techniques [*Roberts*, 2000; *Nakariakov and Ofman*, 2001; *Aschwanden et al*., 2002; *Morton et al*., 2015]. This is significant in that the transverse nature of the waves yields the plane-of-sky component of the magnetic field which is complementary to the line-of-sight component provided by the Zeeman measurements; the combination could provide the complete vector magnetic field in the corona. Also, coronal seismology offers the possibility of measuring flows in the corona. Such measurements in open field regions could provide boundary conditions for solar wind prediction models.

Rapidly accelerating and expanding CMEs are more likely to produce large solar energetic particle events [*Schwadron et al*., 2015]. These CMEs drive shocks in the very low corona where densities are orders of magnitude higher than in the outer corona observed by space-based coronagraphs. Low coronal observations from the COSMO K-Cor will fill the gap between space-based observations of the low corona in EUV and X-ray and the outer corona provided by SOHO/LASCO and STEREO. CME accelerations and expansion rates can be determined using observations from the COSMO K-Cor to improve understanding of SEP production by CME-driven shocks.

The COSMO instruments will provide an unprecedented opportunity for studying the chromospheric and coronal magnetic field evolution that leads to energy storage and explosive release into the heliosphere, thus supporting the development of a predictive capability for solar eruptions. One reason that white light data has proved to be a useful synoptic observation is that the forward problem relating observed white light to coronal density is well specified. Although not as simple, the forward problem relating COSMO LC observables to coronal magnetic field and plasma properties is also well understood and has been incorporated by *Judge and Casini* [2001] into the "CLE" polarimetry synthesis code. This code is a component of the FORWARD SolarSoft IDL package [*Gibson*, 2015b], which also utilizes the CHIANTI database to model all of the COSMO LC lines as well as K-Cor type white light data. Thus, FORWARD can create synthetic data from any magnetic extrapolation or MHD simulation of the solar corona that are directly comparable to COSMO LC and K-Cor observations. These can be used to validate model predictions and/or to enable forward fitting for reconstruction of the magnetothermal environment of the solar atmosphere—a required inner boundary condition for space weather models. Recent work demonstrates the utility of forward modeling to probe magnetic structures and differentiate between models, even in the presence of line-of-sight integration issues [*Bak-Steslicka et al*., 2013; *Rachmeler et al*., 2013, 2014; *Jibben et al*., 2016]. The COSMO LC will provide the critical measurements needed to drive global models from qualitative estimates to full-scale predictive capabilities; it will constrain these models with direct determinations of the magnetic field and thermodynamic properties of the corona.

COSMO data will be used to drive and test the development of the Space Weather Modeling Framework (SWMF) model. SWMF consists of a suite of modular computer codes developed at the University of Michigan that enables space weather forecasting [*Toth et al*., 2012]. SWMF modules include first-principle 3-D models of the solar atmosphere, the inner Heliosphere, the outer Heliosphere, and planetary magnetospheres and ionospheres. The coupled solar corona model/inner heliosphere model (Alfvén Wave Solar Model, AWSoM) [*van der Holst et al*., 2014; *Meng et al*., 2015] includes the chromosphere, transition region

and low corona in a self-consistent, multispecies, multitemperature approach. This model treats ions and electrons as two separate species with the same bulk velocity, collisionally coupled thermodynamics, and heat conduction applied only to electrons; dissipation of Alfvén waves heats the corona and accelerates the solar wind by the Alfvén wave pressure gradient. Two types of dissipation processes are taken into account: (i) Kolmogorov-type dissipation [*Hollweg*, 1986] and (ii) counterpropagating wave dissipation [*Isenberg*, 1987].

Currently, the AWSoM model relies on boundary conditions specified in the upper chromosphere: uniform, outward propagating Alfvén wave energy, density at the solar surface, and synoptic magnetograms to specify the radial magnetic field at the inner boundary. However, no real observational constraint is taken for the coronal magnetic field, and average values of the wave density at the solar surface are taken from the observations of *McIntosh et al.* [2011], which will be different under different conditions of the solar atmosphere. COSMO observations will provide measurements of Alfvén wave properties and coronal magnetic field properties that will be used in two ways: to provide more realistic boundary conditions and to test predictions with observations. These will in turn drive further improvement to the AWSoM model in order to predict both the background solar wind and corotating interaction region properties, as well as CME propagation and arrival time at Earth.

7. COSMO Implementation and Status

COSMO will be designed and built by a group of partner institutions including the National Center for Atmospheric Research, the University of Michigan, the University of Hawaii, George Mason University, and the Harvard Smithsonian Center for Astrophysics along with industry partners. Community input for the COSMO project is provided by the COSMO Steering Committee composed of a broad base of scientists from the international community; they have set instrument requirements through the development of a set of use cases for the instruments.

An extensive evaluation of the observing conditions at Haleakala and Mauna Loa Hawaii as they pertain to COSMO was performed [*Tomczyk et al*., 2015]. This evaluation determined that both sites meet the COSMO requirements, with a slight preference for Mauna Loa. The COSMO LC will reside in a dome (shown in Figure 1), while the K-Cor and ChroMag instruments will reside on a solar pointed platform (spar) in a nearby smaller dome. The spar has eight sides on which to place instruments. The unused space on this pointing platform will be made available to deploy instruments developed by members of the scientific community.

Data obtained by the COSMO instruments will be converted into standard data products and served to the community at the COSMO Data Center. COSMO will have an open data policy, providing all observational data and models to the scientific community.

The COSMO instruments have been developed to a high level of technical readiness. The K-Cor instrument has been completed and has been operational since September 2013. The LC has finished its preliminary design phase and the feasibility of constructing the large refractive coronagraph is documented with engineering studies, preliminary designs, and vendor quotes for all major components. The measurement methodologies for the COSMO LC have been demonstrated with prototype instruments [*Lin et al*., 2004; *Tomczyk et al*., 2008]. The Coronal Multichannel Polarimeter instrument [*Tomczyk et al*., 2008] is currently undergoing an upgrade that will increase the field of view to 1°, to match that for the LC, and will employ a five-stage tunable birefringent filter with Lithium Niobate waveplates [*Landi et al*., 2016] that will demonstrate technology to be used in the COSMO LC tunable filter. The ChroMag instrument is now in the development phase with observations from the ChroMag prototype expected in 2016.

8. Summary

COSMO will provide a unique combination of magnetic field, density, temperature, and velocity observations in the corona and chromosphere that will transform our understanding of the processes responsible for solar activity and the generation of space weather. We have described how the choice and design of the instruments of COSMO are driven by science requirements and discussed applications and methodologies that are being developed in anticipation of its novel and comprehensive observations. The large field of view,

synoptic observations from COSMO will be complementary to the high spatial resolution, small field-of-view observations that will be obtained by the DKIST. The visible and IR diagnostics provided by COSMO are likewise complementary to radio techniques. The COSMO observations will enhance the value of data collected by other observatories on the ground and in space. COSMO will have an open data policy and provide an observing platform for community developed instruments. The maturity of COSMO and its scientific relevance was reflected by the endorsement of the COSMO project as a high priority in the latest Heliophysics Decadal Survey [*Baker et al*., 2013].

Acknowledgments
This work was supported by the National Science Foundation (NSF) through the NCAR strategic initiative process, the NCAR directors reserve, and base funding to HAO. The authors thank two anonymous referees, R. Morton, and JGR Editors Yuming Wang and Mike Liemohn for thoughtful feedback on the manuscript. S.E.G. thanks K.D. Leka for useful discussions and acknowledges support from the Air Force Office of Space Research, FA9550-15-1-0030. E.L. and S.T. acknowledge support from NSF grant AGS-1408789. Key elements of the COSMO LC design were provided by Zhen Wu and Haiying Zhang with support from the Nanjing Institute of Astronomical Optics and Technology. The authors would like to acknowledge HAO engineers Gregory L. Card, David F. Elmore, Dennis Gallagher, Rob Graves, Don Kolinski, Brandon Larson, Alice Lecinski, Peter G. Nelson, Philip Oakley, Scott Sewell, Rich Summers, and Lee Sutherland for their dedicated work in developing the COSMO instruments and the machine shop facility at NCAR for fabrication. The National Center for Atmospheric Research is sponsored by the National Science Foundation. Data and supporting materials can be found at http://www2.hao.ucar.edu/cosmo.

References

Alissandrakis, C. A., and F. Chiuderi-Drago (1995), Coronal magnetic fields from Faraday rotation observations, *Sol. Phys.*, *160*, 171–179, doi:10.1007/BF00679103.

Antiochos, S. K., C. R. DeVore, and J. A. Klimchuk (1999), A model for solar coronal mass ejections, *Astrophys. J.*, *510*, 485–493, doi:10.1086/306563.

Aschwanden, M. J., B. de Pontieu, C. J. Schrijver, and A. M. Title (2002), Transverse oscillations in coronal loops observed with TRACE II. Measurements of geometric and physical parameters, *Sol. Phys.*, *206*(1), 99–132, doi:10.1023/A:1014916701283.

Aschwanden, M. J., A. Winebarger, D. Tsiklauri, and H. Peter (2007), The coronal heating paradox, *Astrophys. J.*, *659*, 1673, doi:10.1086/513070.

Baker, D. N., A. Charo, and T. Zurbuchen (2013), Science for a technological society: The 2013–2022 decadal survey in solar and space physics, *Space Weather*, *11*, 50–51, doi:10.1002/swe.20022.

Bak-Steslicka, U., S. E. Gibson, Y. Fan, C. Bethge, B. Forland, and L. A. Rachmeler (2013), The magnetic structure of solar prominence cavities: New observational signature revealed by coronal magnetometry, *Astrophys. J. Lett.*, *770*(2), L28.

Bastian, T. S. (2003), The frequency agile solar radiotelescope, *Adv. Space Res.*, *32*(12), 2705–2714, doi:10.1016/S0273-1177(03)00903-7.

Bogod, V. M., and G. B. Gelfreikh (1980), Measurements of the magnetic field and the gradient of temperature in the solar atmosphere above a flocculus using radio observations, *Sol. Phys.*, *67*, 29–40, doi:10.1007/BF00146680.

Bommier, V., E. Landi Degl'Innocenti, J. L. Leroy, and S. Sahal-Brechot (1994), Complete determination of the magnetic field vector and of the electron density in 14 prominences from linear polarization measurements in the HeI D_3 and Hα lines, *Sol. Phys.*, *154*, 231, doi:10.1007/BF00681098.

Brosius, J. W., and S. M. White (2006), Radio measurements of the height of strong coronal magnetic fields above sunspots at the solar limb, *Astrophys. J.*, *641*, L69–L72, doi:10.1086/503774.

Brueckner, G. E., et al. (1995), The Large Angle Spectroscopic Coronagraph (LASCO), *Sol. Phys.*, *162*, 357, doi:10.1007/BF00733434.

Canfield, R. C., H. S. Hudson, and D. E. McKenzie (1999), Sigmoidal morphology and eruptive solar activity, *Geophys. Res. Lett.*, *26*, 627–630, doi:10.1029/1999GL900105.

Casini, R. (2007), Prominence and filament magnetometry simulations, *COSMO Tech. Note 12*, High Alt. Obs., Boulder, Colo.

Casini, R., A. López Ariste, S. Tomczyk, and B. W. Lites (2003), Magnetic maps of prominences from full stokes analysis of the He I D_3 line, *Astrophys. J.*, *598*, L67, doi:10.1086/380496.

Cavallini, F. (2006), IBIS: A new post-focus instrument for solar imaging spectroscopy, *Sol. Phys.*, *236*, 415, doi:10.1007/s11207-006-0103-8.

Culhane, J. L., et al. (2007), The EUV imaging spectrometer for Hinode, *Sol. Phys.*, *243*, 19–61, doi:10.1007/s01007-007-0293-1.

De Pontieu, B., et al. (2007), Chromospheric alfvénic waves strong enough to power the solar wind, *Science*, *318*, 1574, doi:10.1126/science.1151747.

De Pontieu, B., A. M. Title, and J. R. Lemen (2014), The Interface Region Imaging Spectrograph (IRIS), *Sol. Phys.*, *289*, 2733–2779, doi:10.1007/s11207-014-0485-y.

DeRosa, M. L., et al. (2009), A critical assessment of nonlinear force-free field modeling of the solar corona for active region 10953, *Astrophys. J.*, *696*, 1780, doi:10.1088/0004-637X/696/2/1780.

de Wijn, A. G., J. T. Burkepile, S. Tomczyk, P. Nelson, P. Huang, and D. Gallagher (2012), Stray light and polarimetry considerations for the COSMO K-coronagraph, *Proc. SPIE*, *8444*, doi:10.1117/12.926511.

de Wijn, A. G., C. Bethge, S. Tomczyk, and S. W. McIntosh (2014), The chromosphere and prominence magnetometer, *Proc. SPIE*, *8446*, 844678, doi:10.1117/12.926395.

Dulk, G. A., and D. J. McLean (1978), Coronal magnetic fields, *Sol. Phys.*, *57*, 279–295, doi:10.1007/BF00160102.

Elmore, D. F., J. T. Burkepile, J. A. Darnell, A. R. Lecinski, and A. L. Stanger (2003), Calibration of a ground-based solar coronal polarimeter, *Proc. SPIE*, *4843*, 66–75, doi:10.1117/12.459279.

Evans, J. W. (1949), The birefringent filter, *J. Opt. Soc. Am.*, *39*, 229, doi:10.1364/JOSA.39.000229.

Fan, Y. (2011), An MHD model of the December 13 2006 eruptive flare, *Astrophys. J.*, *740*, 68, doi:10.1088/0004-637X/740/2/68.

Fisher, R. R., R. H. Lee, R. M. MacQueen, and A. I. Poland (1981), New Mauna Loa coronagraph systems, *Appl. Opt.*, *20*, 1094–1101, doi:10.1364/AO.20.001094.

Forland, B. C., S. E. Gibson, J. B. Dove, L. A. Rachmeler, and Y. Fan (2013), Coronal cavity survey: Morphological clues to eruptive magnetic topologies, *Sol. Phys.*, *288*(2), 603–615, doi:10.1007/s11207-013-0361-1.

Frazin, R. A., A. M. Vásquez, F. Kamalabadi, and H. Park (2007), Three-dimensional tomographic analysis of a high-cadence LASCO-C2 polarized brightness sequence, *Astrophys. J.*, *671*(2), L201–L204, doi:10.1086/525017.

Gary, D. E., and G. J. Hurford (1994), Coronal temperature, density and magnetic field maps of a solar active region using the Owens Valley solar array, *Astrophys. J.*, *420*, 903–912, doi:10.1086/173614.

Gibson, S. (2015a), Coronal cavities: Observations and implications for the magnetic environment of prominences, in *Solar Prominences*, *Astrophys. and Space Sci. Libr.*, vol. 415, 323 pp., Springer, Cham, Switzerland.

Gibson, S. (2015b), Data-model comparison using FORWARD and CoMP, *Proc. Int. Astron. Union*, *305*, 245–250.

Gibson, S. E., et al. (2002), The structure and evolution of a sigmoidal active region, *Astrophys. J.*, *574*, 1021, doi:10.1086/341090.

Gopalswamy, N. (2015), The dynamics of eruptive prominences, in *Solar Prominences*, *ASSL*, vol. 415, edited by J. C. Vial and O. Engvold, pp. 381, Springer, Switzerland.

Gray, L. J., et al. (2010), Solar influence on climate, *Rev. Geophys.*, *48*, RG4001, doi:10.1029/2009RG000282.

Grebinskij, A., V. Bogod, G. Gelfreikh, S. Urpo, S. Pohjolainen, and K. Shibasaki (2000), Microwave tomography of solar magnetic fields, *Astron. Astrophys. Suppl. Ser.*, *144*, 169–180, doi:10.1051/aas:2000202.

Habbal, S. R., M. Druckmüller, H. Morgan, A. Ding, J. Johnson, H. Druckmüllerová, A. Daw, M. B. Arndt, M. Dietzel, and J. Saken (2011), Thermodynamics of the solar corona and evolution of the solar magnetic field as inferred from the total solar eclipse observations of 2010 July 11, *Astrophys. J.*, *734*, 120–127, doi:10.1088/0004-637X/734/2/120.

Hale, G. E. (1908), On the probable existence of a magnetic field in sun-spots, *Astrophys. J.*, *28*, 315, doi:10.1086/141602.

Handy, B. N., et al. (1999), The transition region and coronal explorer, *Sol. Phys.*, *187*, 229–260, doi:10.1023/A:1005166902804.

Harvey, J. W., F. Hill, R. P. Hubbard, J. R. Kennedy, and J. W. Leibacher (1996), The Global Oscillation Network Group (GONG) project, *Science*, *272*(5266), 1284–1286, doi:10.1126/science.272.5266.1284.

Hollweg, J. V. (1986), Transition region, corona, and solar wind in coronal holes, *J. Geophys. Res.*, *91*, 4111–4125, doi:10.1029/JA091iA04p04111.

Hood, A. W., and E. R. Priest (1981), Critical conditions for magnetic instabilities in force-free coronal loops, *Geophys. Astrophys. Fluid Dyn.*, *17*, 297, doi:10.1080/03091928108243687.

Howard, R. A., N. R. Sheeley, D. J. Michels, and M. J. Koomen (1985), Coronal mass ejections: 1979–1981, *J. Geophys. Res.*, *90*, 8173–8191, doi:10.1029/JA090iA09p08173.

Hundhausen, A. J. (1993), Sizes and locations of coronal mass ejections – SMM observations from 1980 and 1984-1989, *J. Geophys. Res.*, *98*, 13,177–13,200, doi:10.1029/93JA00157.

Isenberg, P. A. (1987), Energy diffusion of pickup ions upstream of comets, *J. Geophys. Res.*, *92*, 8795–8799, doi:10.1029/JA092iA08p08795.

Iucci, N., et al. (2006), Spacecraft operational anomalies and space weather impact hazards, *Adv. Space Res.*, *37*, 184, doi:10.1016/j.asr.2005.03.028.

Jacquinot, P. (1954), The luminosity of spectrometers with prisms, gratings, or Fabry Perot etalons, *JOSA, 44*, 761.

Jensen, E. A., M. M. Bisi, A. R. Breen, C. Heiles, T. Minter, and F. Vilas (2013), Measurements of Faraday rotation through the solar corona during the 2009 solar minimum with the Messenger spacecraft, *Sol. Phys.*, *285*, 83–95, doi:10.1007/s11207-012-0213-4.

Jibben, P. R., K. K. Reeves, and Y. Su (2016), Evidence for a magnetic flux rope in observations of a solar prominence-cavity system, *Front. Astron. Space Sci.*, *3*, 10, doi:10.3389/fspas.2016.00010.

Judge, P. G., and R. Casini (2001), A synthesis code for forbidden coronal lines, advanced solar polarimetry—Theory, observation, and instrumentation, in *20TH NSO/Sac Summer Workshop, ASP Conference Proceedings*, vol. 236, edited by M. Sigwarth, 503 pp., Astron. Soc. of the Pac., San Francisco, Calif.

Judge, P. G., R. Casini, S. Tomczyk, D. P. Edwards, and E. Francis (2001), Coronal magnetometry: A feasibility study, *NCAR Tech. Rep. NCAR/TN-446-STR*.

Kahler, S. W. (1992), Solar flares and coronal mass ejections, *Annu. Rev. Astron. Astrophys.*, *30*, 113–141, doi:10.1146/annurev.aa.30.090192.000553.

Keil, S. L., et al. (2003), Design and development of the Advanced Technology Solar Telescope (ATST), *Proc. SPIE*, *4853*, 240–251.

Keller, C. U., J. W. Harvey, and M. S. Giampapa (2003), SOLIS: An innovative suite of synoptic instruments, *Proc. SPIE*, *4853*, 194–204.

Kliem, B., and T. Török (2006), Torus instability, *Phys. Rev. Lett.*, *96*(25), 255002, doi:10.1103/PhysRevLett.96.255002.

Klimchuk, J. A. (2006), On solving the coronal heating problem, *Sol. Phys.*, *234*, 41, doi:10.1007/s11207-006-0055-z.

Kobayashi, K., et al. (2014), The High-Resolution Coronal Imager (Hi-C), *Sol. Phys.*, *289*, 4393–4412, doi:10.1007/s11207-014-0544-4.

Kramar, M., B. Inhester, and S. K. Solanki (2006), Vector tomography for the coronal magnetic field. I. Longitudinal Zeeman effect measurements, *Astron. Astrophys.*, *456*(2), 665–673, doi:10.1051/0004-6361:20064865.

Kramar, M., B. Inhester, H. Lin, and J. Davila (2013), Vector tomography for the coronal magnetic field. II. Hanle effect measurements, *Astrophys. J.*, *775*(1), 25, doi:10.1088/0004-637X/775/1/25.

Kramar, M., V. Airepetian, Z. Mikic, and J. Davila (2014), 3D Coronal Density Reconstruction and Retrieving the Magnetic Field Structure during Solar Minimum, *Sol. Phys.*, *289*(8), 2927–2944, doi:10.1007/s11207-014-0525-7.

Kramar, M., H. Lin, and S. Tomczyk (2016), Direct observation of solar coronal magnetic fields by vector tomography of the coronal emission line polarizations, *Astrophys. J. Lett.*, *819*(2), L36–L41, doi:10.3847/2041-8205/819/2/L36.

Lambour, R. L., A. J. Coster, R. Clouser, L. E. Thornton, J. Sharma, and T. A. Cott (2003), Operational impacts of space weather, *Geophys. Res. Lett.*, *30*(3), 1136, doi:10.1029/2002GL015168.

Landi, E., J. C. Raymond, M. P. Miralles, and H. Hara (2010), Physical conditions in a coronal mass ejection from Hinode, STEREO, and SOHO observations, *Astrophys. J.*, *711*, 75, doi:10.1088/0004-637X/711/1/75.

Landi, E., S. R. Habbal, and S. Tomczyk (2016), Coronal plasma diagnostics from ground-based observations, *J. Geophys. Res. Space Physics*, *122*, doi:10.1002/2016JA022598, in press.

Lemen, J. R., et al. (2012), The Atmospheric Imaging Assembly (AIA) on the Solar Dynamics Observatory (SDO), *Sol. Phys.*, *275*, 17–40, doi:10.1007/s11207-011-9776-8.

Leroy, J. L., V. Bommier, and S. Sahal-Bréchot (1984), New data on the magnetic structure of quiescent prominences, *Astron. Astrophys.*, *131*, 33.

Lin, H., J. R. Kuhn, and R. Coulter (2004), Coronal magnetic field measurements, *Astrophys. J.*, *613*, L177, doi:10.1086/425217.

Low, B. C. (1994), Magnetohydrodynamic processes in the solar corona: Flares, coronal mass ejections and magnetic helicity, *Phys. Plasmas*, *1*, 1684, doi:10.1063/1.870671.

Low, B. C. (2001), Coronal mass ejections, magnetic flux ropes and solar magnetism, *J. Geophys. Res.*, *106*, 25,141–25,164, doi:10.1029/2000JA004015.

Lyot, B. (1933), Optical apparatus with wide field using interference of polarized light, *C. R. Acad. Sci. Ser. A*, *197*, 1593.

MacQueen, R. M., J. T. Burkepile, T. E. Holzer, A. L. Stanger, and K. E. Spence (2001), Solar coronal brightness changes and mass ejections during solar cycle 22, *Astrophys. J.*, *549*, 1175, doi:10.1086/319464.

Malanushenko, A., C. J. Schrijver, M. L. DeRosa, M. S. Wheatland, and S. A. Gilchrist (2012), Guiding nonlinear force-free modeling using coronal observations: First results using a quasi-grad-rubin scheme, *Astrophys. J.*, *756*(2), 153, doi:10.1088/0004-637X/756/2/153.

McIntosh, S. W., B. De Pontieu, M. Carlsson, V. Hansteen, P. Boerner, and M. Goossens (2011), Alfvénic waves with sufficient energy to power the quiet solar corona and fast solar wind, *Nature*, *475*, 477, doi:10.1038/nature10235.

Meng, X., B. van der Holst, G. Toth, and T. I. Gombosi (2015), Alfvén wave solar model (AWSoM): Proton temperature anisotropy and solar wind acceleration, *Mon. Not. R. Astron. Soc.*, *454*, 3697, doi:10.1093/mnras/stv2249.

Merenda, L., J. Trujillo Bueno, E. Landi Degl'Innocenti, and M. Collados (2006), Determination of the magnetic field vector via the Hanle and Zeeman effects in the He I λ10830 multiplet: Evidence for nearly vertical magnetic fields in a polar crown prominence, *Astrophys. J.*, *642*, 554, doi:10.1086/501038.

Morton, R. J., and J. A. McLaughlin (2013), Hi-C and AIA observations of transverse magnetohydrodynamic waves in active regions, *Astron. Astrophys.*, *553*, L10, doi:10.1051/0004-6361/201321465.

Morton, R. J., S. Tomczyk, and R. Pinto (2015), Investigating Alfvénic wave propagation in coronal open-field regions, *Nat. Commun.*, *6*, 7813, doi:10.1038/ncomms8813.
Nakariakov, V. M., and L. Ofman (2001), Determination of the coronal magnetic field by coronal loop oscillations, *Astron. Astrophys.*, *372*, L53–L56, doi:10.1051/0004-6361:20010607.
Nelson, P. G., S. Tomczyk, D. F. Elmore, and D. J. Kolinski (2008), The feasibility of large refracting telescopes for solar coronal research, *Proc. SPIE*, *7012*, 701231–701231-12, doi:10.1117/12.789494.
Orozco Suarez, D., A. Asensio Ramos, and J. Trujillo Bueno (2014), The magnetic field configuration of a solar prominence inferred from spectropolarimetric observations in the He I 10830 Å triplet, *Astron. Astrophys.*, *566*, A46, doi:10.1051/0004-6361/201322903.
Paletou, F., A. López Ariste, V. Bommier, and M. Semel (2001), Full-stokes spectro-polarimetry of solar prominences, *Astron. Astrophys.*, *375*, L39, doi:10.1051/0004-6361:20010927.
Penn, M. J., H. Lin, S. Tomczyk, D. F. Elmore, and P. G. Judge (2004), Background induced measurement errors of the coronal intensity, density, velocity and magnetic field, *Sol. Phys.*, *222*, 61–78, doi:10.1023/B:SOLA.0000036850.34404.5f.
Pizzo, V., G. Millward, A. Parsons, D. Biesecker, S. Hill, and D. Odstrcil (2011), Wang-Sheeley-Arge-Enlil cone model transitions to operations, *Space Weather*, *9*, S03004, doi:10.1029/2011SW000663.
Plowman, J. (2014), Single-point inversion of the coronal magnetic field, *Astrophys. J.*, *792*(1), 23, doi:10.1088/0004-637X/792/1/23.
Pulkkinen, T. (2007), Space weather: Terrestrial perspective, *Living Rev. Sol. Phys.*, *4*(1), 1.
Querfeld, C. W., L. L. House, R. N. Smartt, V. Bommier, and E. Landi Degl'Innocenti (1985), Vector magnetic fields in prominences. II—HeI D3 stokes profiles analysis for two quiescent prominences, *Sol. Phys.*, *96*, 277, doi:10.1007/BF00149684.
Rachmeler, L. A., S. E. Gibson, J. B. Dove, C. R. DeVore, and Y. Fan (2013), Polarimetric properties of flux ropes and sheared arcades in coronal prominence cavities, *Sol. Phys.*, *288*, 617, doi:10.1007/s11207-013-0325-5.
Rachmeler, L. A., S. J. Platten, C. Bethge, D. B. Seaton, and A. R. Yeates (2014), Observations of a hybrid double-streamer/pseudostreamer in the solar corona, *Astrophys. J. Lett.*, *787*, L3, doi:10.1088/2041-8205/787/1/L3.
Roberts, B. (2000), Waves and oscillations in the corona, *Sol. Phys.*, *193*, 139–152, doi:10.1023/A:1005237109398.
Roussev, I. I., T. G. Forbes, T. I. Gombosi, I. V. Sokolov, D. L. DeZeeuw, and J. Birn (2003), A three-dimensional flux rope model for coronal mass ejections based on a loss of equilibrium, *Astrophys. J.*, *588*(1), L45–L48, doi:10.1086/375442.
Savcheva, A., and A. van Ballegooijen (2009), Nonlinear force-free modeling of a long-lasting coronal sigmoid, *Astrophys. J.*, *703*(2), 1766–1777, doi:10.1088/0004-637X/703/2/1766.
Scharmer, G. B. (2006), Comments on the optimization of high resolution Fabry-Perot Filtergraphs, *Astron. Astrophys.*, *447*, 1111–1120, doi:10.1051/0004-6361:20052981.
Scherrer, P. H., J. Schou, R. I. Bush, A. G. Kosovichev, and R. S. Bogart (2012), The Helioseismic and Magnetic Imager (HMI) Investigation for the Solar Dynamics Observatory (SDO), *Sol. Phys.*, *275*, 207, doi:10.1007/s11207-011-9834-2.
Schmieder, B., L. van Driel-Gesztelyi, G. Aulanier, P. Démoulin, B. Thompson, C. de Forest, J. E. Wiik, C. Saint Cyr, and J. C. Vial (2002), Relationships between CMEs and prominences, *Adv. Space Res.*, *29*, 1451, doi:10.1016/S0273-1177(02)00211-9.
Schmieder, B., H. Tian, T. Kucera, A. Lopez Ariste, N. Mein, P. Mein, K. Dalmasse, and L. Golub (2014), Open questions on prominences from coordinated observations by IRIS, Hinode, SDO/AIA, THEMIS, and the Meudon/MSDP, *Astron. Astrophys.*, *569*, A85, doi:10.1051/0004-6361/201423922.
Schrijver, C. J. (2015), Socio-economic hazards and impacts of space weather: The important range between mild and extreme, *Space Weather*, *13*, 524–528, doi:10.1002/2015SW001252.
Schrijver, C. J., et al. (2008), Nonlinear force-free field modeling of a solar active region around the time of a major flare and coronal mass ejection, *Astrophys. J.*, *675*(2), 1637–1644, doi:10.1086/527413.
Schwadron, N. A., et al. (2015), Particle acceleration at low coronal compression regions and shocks, *Astrophys. J.*, *810*, 97, doi:10.1088/0004-637X/810/2/97.
St. Cyr, O. C., J. T. Burkepile, A. J. Hundhausen, and A. R. Lecinski (1999), A comparison of ground-based and spacecraft observations of coronal mass ejections from 1980–1989, *J. Geophys. Res.*, *104*, 12,493–12,506, doi:10.1029/1999JA900045.
Thompson, W. T., et al. (2003), The COR1 inner coronagraph for STEREO-SECCHI, *Proc. SPIE*, *4853*, 1–11.
Tian, H., S. Tomczyk, S. W. McIntosh, C. Bethge, G. de Toma, and S. E. Gibson (2013), Observations of coronal mass ejections with the coronal multichannel polarimeter, *Sol. Phys.*, *288*(2), 637–650, doi:10.1007/s11207-013-0317-5.
Tomczyk, S. (2015), Measurement errors for coronal magnetic field parameters, *COSMO Tech. Note 1*.
Tomczyk, S., and S. W. McIntosh (2009), Time-distance seismology of the solar corona with CoMP, *Astrophys. J.*, *697*, 1384–1391, doi:10.1088/0004-637X/697/2/1384.
Tomczyk, S., S. W. McIntosh, S. L. Keil, P. G. Judge, T. Schad, D. H. Seeley, and J. Edmonson (2007), Alfvén waves in the solar corona, *Science*, *317*, 1192, doi:10.1126/science.1143304.
Tomczyk, S., G. L. Card, T. Darnell, D. F. Elmore, R. Lull, P. G. Nelson, K. V. Streander, J. Burkepile, R. Casini, and P. Judge (2008), An instrument to measure coronal emission line polarization, *Sol. Phys.*, *247*, 411, doi:10.1007/s11207-007-9103-6.
Tomczyk, S., R. Casini, A. G. De Wijn, and P. G. Nelson (2010), Wavelength-diverse polarization modulators for Stokes polarimetry, *Appl. Opt.*, *49*, 3580, doi:10.1364/AO.49.003580.
Tomczyk, S., P. Oakley, and P. G. Nelson (2015), COSMO large coronagraph site evaluation and selection, COSMO Tech. Note.
Tomczyk, S., S. K. Mathew, and D. Gallagher (2016), Development of a tunable filter for coronal polarimetry, *J. Geophys. Res. Space Physics*, *121*, doi:10.1002/2016JA022682.
Török, T., B. Kliem, and V. S. Titov (2004), Ideal kink instability of a magnetic loop equilibrium, *Astron. Astrophys.*, *413*, L27–L30, doi:10.1051/0004-6361:20031691.
Toth, G., et al. (2012), Adaptive numerical algorithms in space weather modeling, *J. Comput. Phys.*, *231*, 870, doi:10.1016/j.jcp.2011.02.006.
van der Holst, B., S. I. Sokolov, X. Meng, M. Jin, W. B. Manchester IV, G. Tóth, and T. I. Gombosi (2014), Alfvén Wave Solar Model (AWSoM): Coronal Heating, *ApJ*, *782*, 81, doi:10.1088/0004-637X/782/2/81.
Vourlidas, A., S. T. Wu, A. H. Wang, P. Subramanian, and R. A. Howard (2003), Direct detection of a coronal mass ejection-associated shock in Large Angle and Spectrometric Coronagraph Experiment white-light images, *Astrophys. J.*, *598*, 1392, doi:10.1086/379098.
Webb, D. F., and T. A. Howard (2012), Coronal mass ejections: Observations, *Living Rev. Sol. Phys.*, *9*(3), 3, doi:10.12942/lrsp-2012-3.
Wedemeyer, S., et al. (2015), SSALMON—The Solar Simulations for the Atacama Large Millimeter Observatory Network, *Adv. Space Res.*, *56*(12), 2679–2692, doi:10.1016/j.asr.2015.05.027.
White, S. (2005), Radio measurements of coronal magnetic fields, in *Proceedings of the International Scientific Conference on Chromospheric and Coronal Magnetic Fields (ESA SP-596)*, edited by D. E. Innes, A. Lagg, and S. K. Solanki, pp. 89–113, ESA, Noordwijk, Netherlands.

White, S. M., and M. R. Kundu (1997), Radio observations of gyroresonance emission from coronal magnetic fields, *Sol. Phys.*, *174*, 31–52, doi:10.1023/A:1004975528106.

Wiegelmann, T., and T. Sakurai (2012), Solar force-free magnetic fields, *Living Rev. Sol. Phys.*, *9*(5), 5, doi:10.12942/lrsp-2012-5.

Xu, Z., A. Lagg, S. Solanki, and Y. Liu (2012), Magnetic fields of an active region filament from full Stokes analysis of Si I 1082.7 nm and He I 1083.0 nm, *Astrophys. J.*, *749*, 138, doi:10.1088/0004-637X/749/2/138.

Yan, Y., J. Zhang, W. Wang, F. Liu, Z. Chen, and G. Ji (2009), The Chinese spectral radioheliograph—CSRH, *Earth Moon Planets*, *104*(1–4), 97–100, doi:10.1007/s11038-008-9254-y.

Zhang, J., N. Gopalswamy, M. R. Kundu, E. J. Schmahl, and J. R. Lemen (1998), Spatial structure of solar coronal magnetic loops revealed by transient microwave brightenings, *Sol. Phys.*, *182*, 285–298, doi:10.1023/A:1005020207482.

Zhang, J., X. Cheng, and M.-D. Ding (2012), Observation of an evolving magnetic flux rope before and during a solar eruption, *Nat. Commun.*, *3*, 747, doi:10.1038/ncomms1753.